

Interlaminar Tension-Tension Fatigue of Woven Glass Fiber Reinforced Plastic Composite Laminates at Low Temperatures

Fumio Narita*, Chieko Tanaka and Masashi Suzuki

Department of Materials Processing, Graduate School of Engineering, Tohoku University, Sendai 980-8579, Japan

Abstract: Experimentally characterizing the through-thickness tensile behavior of composite laminates is challenging. This paper investigates the through-thickness tensile fatigue behavior of woven glass fiber reinforced plastic (GFRP) composite laminates at low temperatures. Cyclic through-thickness tensile tests were performed with cross specimens at room temperature and liquid nitrogen temperature (77 K), and the maximum interlaminar stress versus number of cycles to failure (S-N curve) was evaluated. The interlaminar tensile fatigue mechanisms of the woven GFRP composite laminates at low temperatures were also discussed. It was shown that resin fracture is dominant at room temperature, and the interface bonding fracture between the fiber and the matrix is dominant at 77K.

Keywords: Cryomechanics, Fatigue test, Fiber reinforced plastic composites, Interlaminar strength, Liquid nitrogen temperature.

INTRODUCTION

Woven GFRP composite laminates are used as electrical, thermal insulation and structural support in superconducting magnets such as the International Thermonuclear Experimental Reactor (ITER) [1]. On the other hand, failure between layers is one of the most critical failure modes in woven composite laminates. Therefore, interlaminar mechanical properties can govern the design of composite structures. Up to now, many studies have been conducted regarding interlaminar shear strength of woven composite laminates. For example, Shindo *et al.* have investigated the interlaminar shear strength of woven GFRP composite laminates [2, 3] and hybrid composite laminates consisting of woven GFRP composites and polyimide films [4, 5] at cryogenic temperature. Takeda *et al.* [6] have examined the shear strength and damage self-sensing of woven CFRP composite laminates at cryogenic temperatures. Recently, it has been clarified that the interlaminar mechanical properties of FRP are improved by the nano-filler in the epoxy matrix. Zeng *et al.* [7, 8] investigated the effect of multi-walled carbon nanotubes (MWCNTs) on the interlaminar fracture toughness in the woven GFRP composite laminates. Tessema *et al.* [9] also researched the effect of the silica nano-particles on the interlaminar shear properties in the woven CFRP composite laminates.

There are only a few studies about interlaminar tensile strength of woven GFRP composite laminates.

ASTM standard test method [10] is used to determine the through-thickness tensile strength and elastic modulus of fiber-reinforced polymer matrix composite materials. A tensile force is applied using adhesively bonded thick metal end tabs. However, since the bond strength of adhesive may be lower than the through-thickness strength of the composite laminates, failures at the adhesive bondline between the composite specimen and the end tabs is one of the drawbacks of this test method. In addition, it is especially difficult to find an adhesive suitable for use at cryogenic temperatures.

Recently, Gerlach *et al.* [11] proposed a cross specimen to characterize the through-thickness tensile properties of three-dimensional (3D) woven carbon fiber reinforced composites. Takeda *et al.* [12] also proposed a cross specimen to investigate interlaminar tensile behavior of woven GFRP composite laminates at cryogenic temperatures. The cross specimen was designed by performing three-dimensional finite element analysis. Static through-thickness tensile tests were performed on woven GFRP composite laminates using this cross specimen, and failure mechanisms were investigated. In the study by Zeng *et al.* [7], it was reported that the interlaminar tensile strength of the woven GFRP composites laminates was enhanced due to the MWCNTs in the matrix. Ranz *et al.* [13] carried out the four point bending tests in accordance with ASTM D 6415 and calculated the interlaminar tensile strength of the woven CFRP composite laminates by the simplified formulation.

In this study, cyclic through-thickness tensile tests were performed to investigate the interlaminar tensile

*Address correspondence to this author at the Department of Materials Processing, Graduate School of Engineering, Tohoku University, Sendai 980-8579, Japan; Tel: +81-22-7342; E-mail: narita@material.tohoku.ac.jp

fatigue mechanisms at low temperatures using the cross specimen.

EXPERIMENTAL PROCEDURE

G-11 woven GFRP laminates were considered in this study. The fiber reinforcement was a plain weave E-glass fabric and the matrix was a bisphenol-A epoxy resin. The overall fiber volume fraction was 39 %. The specimen used was the cross specimen of woven GFRP composite laminates. Figure 1 shows the schematic of the specimen.

Cyclic through-thickness tensile tests were performed with a frequency of 4 Hz and the load ratio (R) was equal to 0.1 at room temperature (RT) and liquid nitrogen temperature (77 K). The maximum applied stress σ_{\max} in the fatigue tests are listed in the Table 1; where σ_B denotes the static failure stress.

RESULTS AND DISCUSSION

Figure 2 shows the fracture location of the specimen at room temperature after the fracture test and fatigue test. In both cases, the failure location was near the center of the specimen, and they were both interlaminar tensile failures. Figure 3(a) shows the

fracture location of the specimen at 77 K after the fracture test. Similar to the results at room temperature, the failure location was near the center of the specimen. On the other hand, Figure 3(b) shows the fracture location of the fatigue test specimen at 77 K. The fracture was seen at the shoulder radius section in some specimens, and delamination occurred in multiply. From the stress distribution data obtained by the finite element analysis [6], it seems that at this location, in addition to the tensile stress in the through-thickness direction, shearing stress also occurred, resulting in complex stress field. Therefore, we defined this specimen as complex stress failure specimen.

Figure 4 shows the maximum interlaminar stress σ_{\max} versus number of cycles to failure N at room temperature and 77 K from the through-thickness tensile failure (circles) and the complex stress failure (triangle). Plots of $N = 10^0$ represent results of the fracture tests. The number of cycles to failure tend to decrease with the increase in maximum interlaminar stress σ_{\max} . Specimens fractured by complex stress failure account for more than 75% of the data at 77 K. Thus, the complex stress field is subject to occur at 77 K. This is due to the thermal stress by the difference of liner expansion coefficient between the fiber and resin.

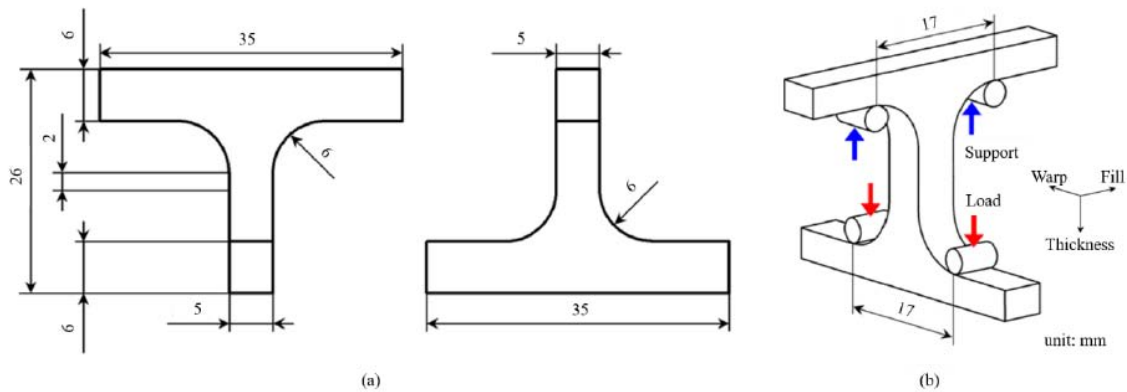


Figure 1: Schematic of (a) size and shape of the cross specimen and (b) through-thickness tensile test set up.

Table 1: Maximum Applied Stress in Fatigue Tests

Temperature	σ_B (MPa)	σ_{\max} (MPa)		
		$\sigma_{\max}/\sigma_B = 0.8$	$\sigma_{\max}/\sigma_B = 0.7$	$\sigma_{\max}/\sigma_B = 0.6$
RT	47.03	37.61	32.92	28.23
77 K	84.24	67.39	58.24	

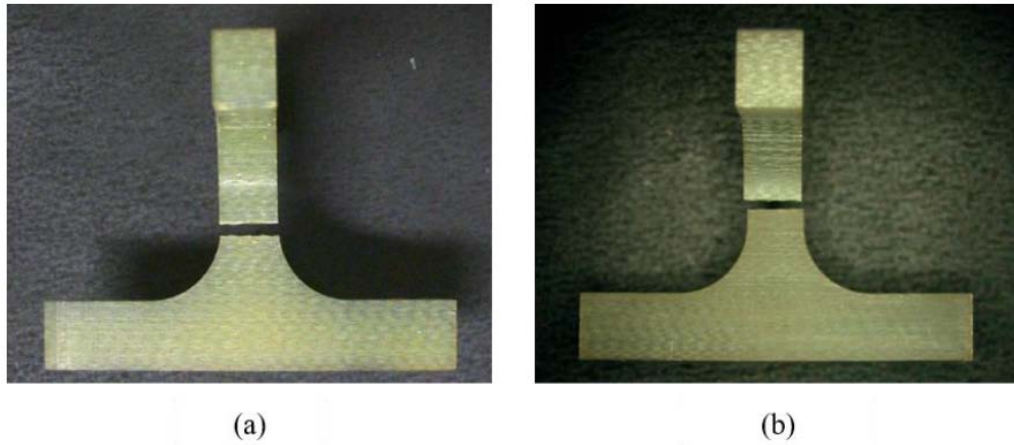


Figure 2: Failure location of cross specimens for (a) fracture test and (b) fatigue test at room temperature.

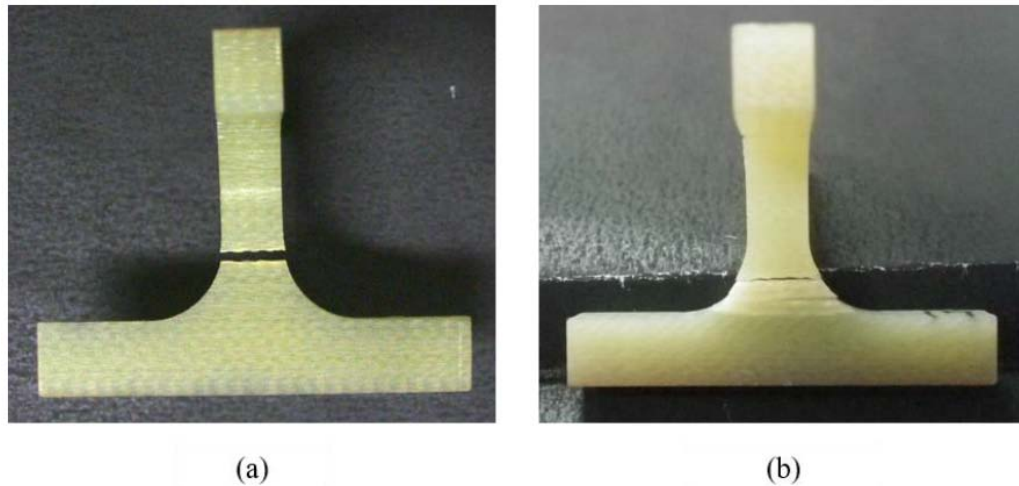


Figure 3: Failure location of cross specimens for (a) fracture test and (b) fatigue test at 77 K.

In addition, the effect of the thermal stress is notable in the fatigue tests.

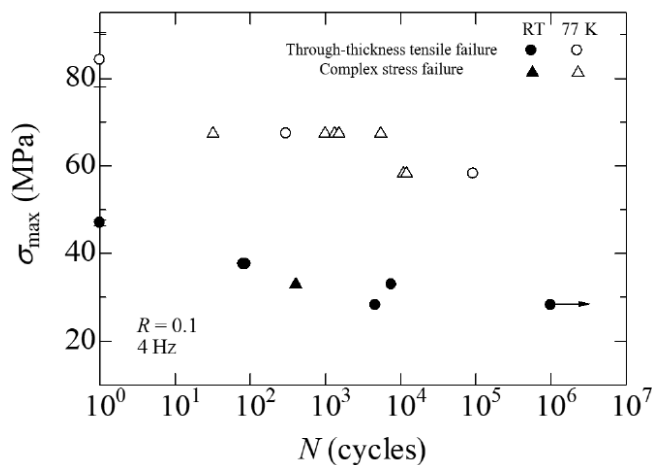


Figure 4: Maximum interlaminar stress versus number of cycles to failure.

Figure 5 shows the fracture surfaces after each test at room temperature. Resin fracture area can be seen. Figure 6 shows the resin fracture area ratio at room temperature. The resin fracture area ratio is defined as the total area of the resin fracture regions divided by the area of the overall fracture surface. There was no remarkable difference between fracture and fatigue tests at room temperature. Figure 7 shows the fracture surfaces after each test at 77 K. Little resin fracture area can be observed for the fatigue tests. Figure 8 shows the resin fracture area ratio at 77 K. The resin fracture area of the specimen after the fatigue tests was found to be smaller than that of the fracture test. It seems that the resin fracture area ratio after the fatigue test was smaller than that of the fracture test because fatigue fracture is dependent on delamination of the fiber/matrix interface bonding. From Figure 5(b) and 7(b), the morphology of the resin was found to be different between room temperature and 77 K. They

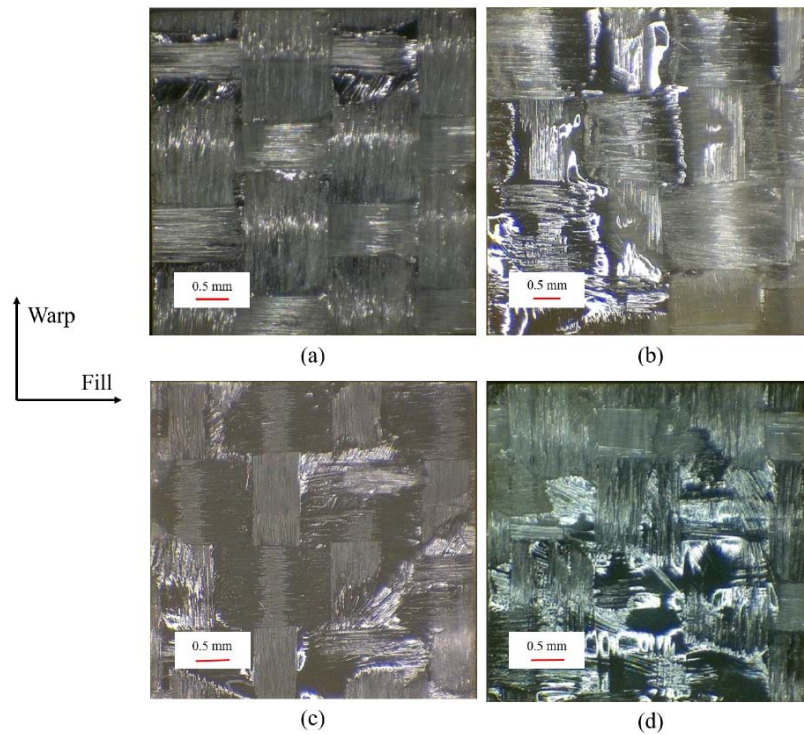


Figure 5: Fracture surface of (a) fracture test and fatigue tests for (b) $\sigma_{max}/\sigma_B = 80\%$, (c) 70% and (d) 60% at room temperature.

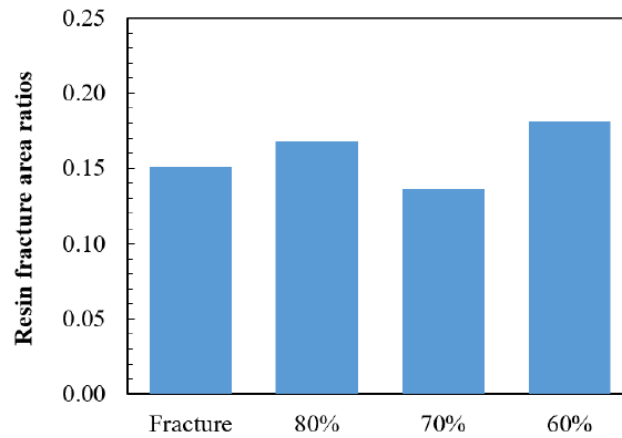


Figure 6: Resin fracture area ratio at room temperature.

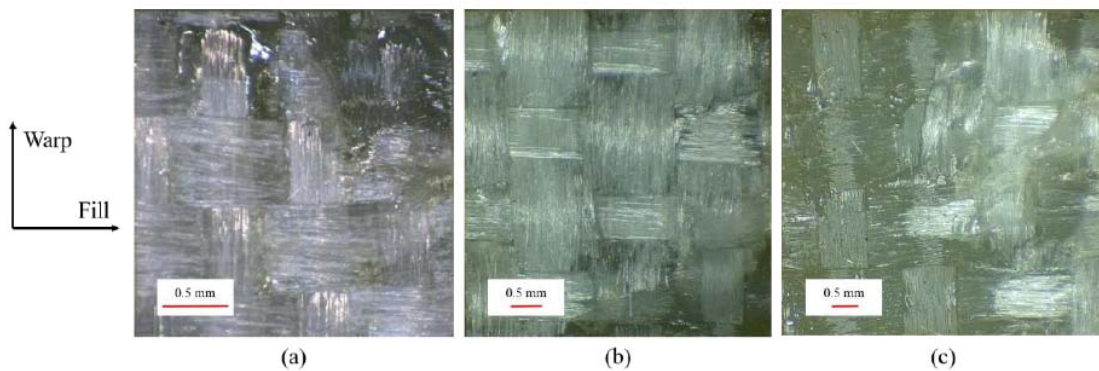


Figure 7: Fracture surface of (a) fracture test and fatigue tests for (b) $\sigma_{max}/\sigma_B=80\%$ and (c) 70% at 77 K.

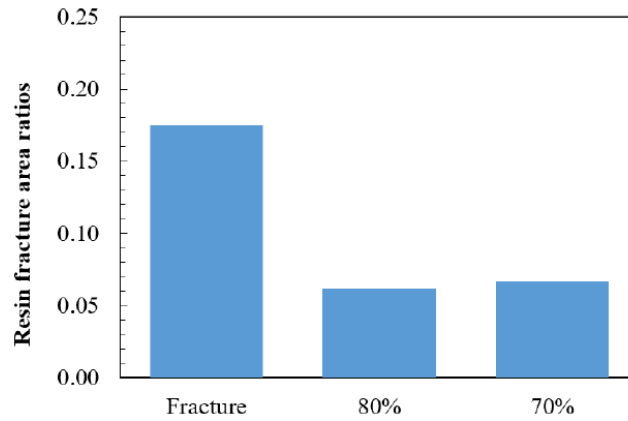


Figure 8: Resin fracture area ratio at 77 K.

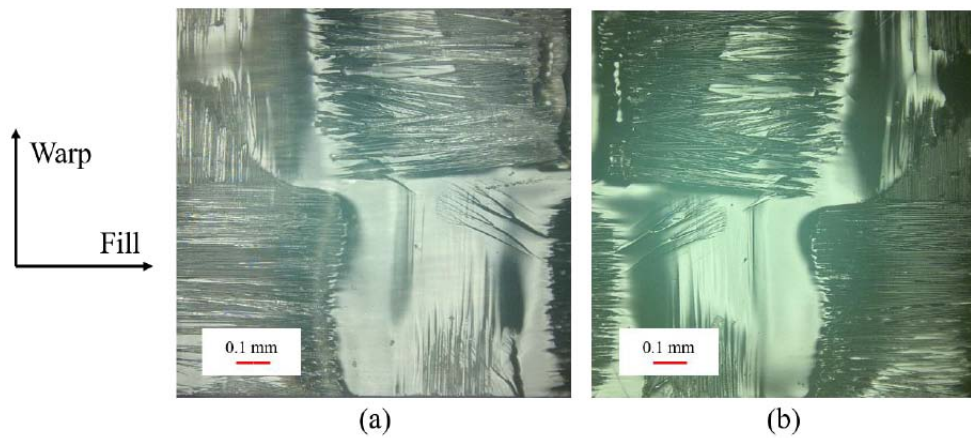


Figure 9: (a) Upper part and (b) lower part for fracture surface of fatigue test at room temperature.

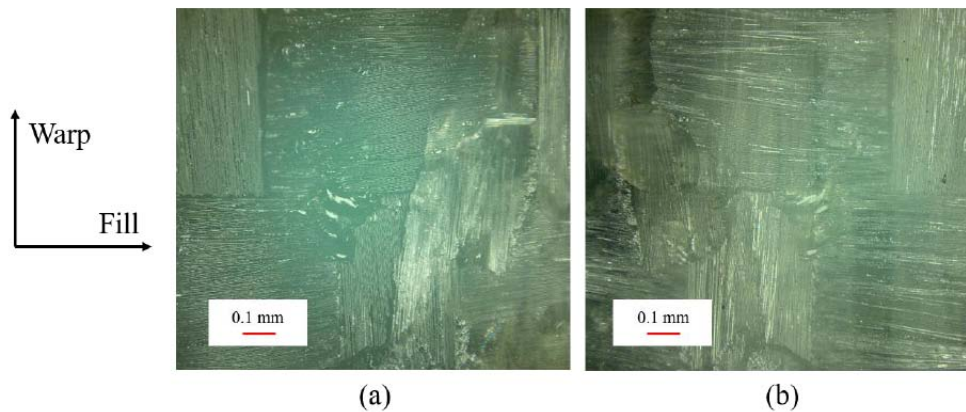


Figure 10: (a) Upper part and (b) lower part for fracture surface of fatigue test at 77 K.

were then observed at high magnification. Figure 9 shows the fracture surface at high magnification of fatigue test at room temperature. They are arranged in line-symmetrically. Regarding upper and lower fracture surfaces, resin remained on corresponding places in both parts. Therefore, it can be concluded that fracture of resin was dominant in fatigue fracture at room temperature. Figure 10 shows the fracture surface at

high magnification of fatigue test at 77 K. Regarding upper and lower fracture surfaces, the area where the resin remained and the area of fiber were found on corresponding places in both parts. Therefore, it can be concluded that the interface bonding fracture between the fiber and the matrix was dominant in fatigue fracture at 77 K.

CONCLUSION

We obtained the maximum interlaminar stress versus number of cycles to failure (S-N curve) of woven GFRP composite laminate at room temperature and 77 K. It became evident that cooling from room temperature to 77K causes an increase in the number of cycles to failure. Furthermore, regarding fatigue failure of woven GFRP composite laminate, it was found that resin fracture is dominant at room temperature, and the interface bonding fracture between the fiber and the matrix is dominant at 77K.

REFERENCES

- [1] N. Mitchell, P. Bauer, D. Bessette, A. Devred, R. Gallix, C. Jong, J. Knaster, B. Lim, A. Sahu, F. Simon. Status of the ITER magnets. *Fusion Eng Des* 84 (2009) 113-121. <https://doi.org/10.1016/j.fusengdes.2009.01.006>
- [2] Y. Shindo, R. Wang, K. Horiguchi, S. Ueda. Theoretical and experimental evaluation of double-notch shear strength of G-10CR glass-cloth/epoxy laminates at cryogenic temperatures. *J Eng Mater Technol* 121 (1999) 367-373. <https://doi.org/10.1115/1.2812388>
- [3] Y. Shindo, R. Wang, K. Horiguchi, Analytical and experimental studies of short-beam interlaminar shear strength of G-10CR glass-cloth/epoxy laminates at cryogenic temperatures. *J Eng Mater Technol* 123 (2001) 112-118 <https://doi.org/10.1115/1.1286235>
- [4] Y. Shindo, T. Takeda, F. Narita, M. Miura, S. Watanabe N. Koizumi, A. Idesaki, K. Okuno. Interlaminar shear properties of composite insulation systems for fusion magnets at cryogenic temperatures. *Cryogenics* 50 (2010) 36-42. <https://doi.org/10.1016/j.cryogenics.2009.10.006>
- [5] M. Miura, Y. Shindo, T. Takeda, F. Narita. Effect of damage on the interlaminar shear properties of hybrid composite laminates at cryogenic temperatures. *Compos Struct* 93 (2010) 124-131 <https://doi.org/10.1016/j.compstruct.2010.06.008>
- [6] T. Takeda, Y. Shindo, T. Fukuzaki, F. Narita. Short beam interlaminar shear behavior and electrical resistance-based damage self-sensing of woven carbon/epoxy composite laminates in a cryogenic environment. *J. Compos. Mater.* 48 (2014) 119-128. <https://doi.org/10.1177/0021998312469240>
- [7] S. Zeng, P. Duan, M. Shen M. Shen, Y. Xue, F. Lu, L. Yang. Interface enhancement of glass fiber fabric/epoxy composites by modifying fibers with functionalized MWCNTs. *Compos. Interfaces* 26 (2019) 291-308. <https://doi.org/10.1080/09276440.2018.1499354>
- [8] S. Zeng, P. Duan, M. Shen M. Shen, X. Lu, Y. Xue, L. Yang. Interlaminar fracture toughness, adhesion and mechanical properties of MWCNTs-glass fiber fabric composites: Effect of MWCNT aspect ratios. *Polymer compos.* in press.
- [9] A. Tessema, W. Mitchell, B. Koohbor, S. Ravindran, M. Van Tooren, A. Kidane. The Effect of nano-fillers on the in-plane and interlaminar shear properties of carbon fiber reinforced composite. *J. Dynamic Behavior Mater* 4 (2018) 296-307. <https://doi.org/10.1007/s40870-018-0166-2>
- [10] ASTM D 7291/D 7291M-07. Standard test method for through-thickness "flatwise" tensile strength and elastic modulus of a fiber-reinforced polymer matrix composite material, *Annual Book of Standards*, vol. 15.03. West Conshohocken, PA.: ASTM International; 2007.
- [11] R. Gerlach, Clive R. Siviour, J. Wiegand, N. Petrinic. In-plane and through-thickness properties, failure modes, damage and delamination in 3D woven carbon fibre composites subjected to impact loading. *Compos. Sci. Technol.* 72 (2012) 397-411. <https://doi.org/10.1016/j.compscitech.2011.11.032>
- [12] T. Takeda, F. Narita, Y. Shindo, K. Sanada. Cryogenic through-thickness tensile characterization of plain woven glass/epoxy composite laminates using cross specimens: Experimental test and finite element analysis. *Compos Part B* 78 (2015) 42-49 <https://doi.org/10.1016/j.compositesb.2015.03.076>
- [13] D. Ranz, J. Cuartero, A. Miravete, R. Miralbes. Experimental research into interlaminar tensile strength of carbon/epoxy laminated curved beams. *Compos. Struct.* 164 (2017) 189-197 <https://doi.org/10.1016/j.compstruct.2016.12.010>

Received on 10-12-2018

Accepted on 20-12-2018

Published on 31-12-2018

DOI: <https://doi.org/10.12974/2311-8717.2018.06.4>© 2018 Narita *et al.*; Licensee Savvy Science Publisher.

This is an open access article licensed under the terms of the Creative Commons Attribution Non-Commercial License (<http://creativecommons.org/licenses/by-nc/3.0/>) which permits unrestricted, non-commercial use, distribution and reproduction in any medium, provided the work is properly cited.